1991-06

Synchronized Oscillations During Cooperative Feature Linking in a Cortical Model of Visual Perception

SYNCHRONIZED OSCILLATIONS DURING COOPERATIVE FEATURE LINKING IN A CORTICAL MODEL OF VISUAL PERCEPTION

Stephen Grossberg and David Somers

June, 1991

Technical Report CAS/CNS–TR–91–019

Boston University Center for Adaptive Systems and
Department of Cognitive and Neural Systems
111 Cummington Street
Boston, MA 02215

SYNCHRONIZED OSCILLATIONS DURING COOPERATIVE FEATURE LINKING IN A CORTICAL MODEL OF VISUAL PERCEPTION

Stephen Grossberg† and David Somers‡
Center for Adaptive Systems
and
Graduate Program in Cognitive and Neural Systems
Boston University
111 Cummington Street
Boston, MA 02215

September, 1990

Neural Networks, in press, 1991

† Supported in part by the Air Force Office of Scientific Research (AFOSR 90-0175), the Army Research Office (ARO DAAL-03-88-K0088), and DARPA (AFOSR 90-0083).

‡ Supported in part by NASA (NGT-50497).

Acknowledgements: The authors wish to thank Carol Yanakakis Jefferson and Cynthia E. Bradford for their valuable assistance in the preparation of the manuscript.

ABSTRACT

A neural network model of synchronized oscillator activity in visual cortex is presented in order to account for recent neurophysiological findings that such synchronization may reflect global properties of the stimulus. In these recent experiments, it was reported that synchronization of oscillatory firing responses to moving bar stimuli occurred not only for nearby neurons, but also occurred between neurons separated by several cortical columns (several *mm* of cortex) when these neurons shared some receptive field preferences specific to the stimuli. These results were obtained not only for single bar stimuli but also across two disconnected, but colinear, bars moving in the same direction. Our model and computer simulations obtain these synchrony results across both single and double bar stimuli. For the double bar case, synchronous oscillations are induced in the region between the bars, but no oscillations are induced in the regions beyond the stimuli. These results were achieved with cellular units that exhibit limit cycle oscillations for a robust range of input values, but which approach an equilibrium state when undriven. Single and double bar synchronization of these oscillators was achieved by different, but formally related, models of preattentive visual boundary segmentation and attentive visual object recognition, as well as nearest-neighbor and randomly coupled models. In preattentive visual segmentation, synchronous oscillations may reflect the binding of local feature detectors into a globally coherent grouping. In object recognition, synchronous oscillations may occur during an attentive resonant state that triggers new learning. These modelling results support earlier theoretical predictions of synchronous visual cortical oscillations and demonstrate the robustness of the mechanisms capable of generating synchrony.

Key Words: vision, visual cortex, oscillations, neural networks, cooperative feature linking.

1. Experimental Background

On the basis of simultaneous, multi-electrode, extra-cellular recordings, two labs (Eckhorn *et al.*, 1988; Gray and Singer, 1989; Gray *et al.*, 1989) have reported stimulus-evoked resonances or synchronized oscillations of 40–60 Hz in the primary visual cortex (Areas 17 and 18) of the cat. Coherence or synchrony of firing activity was found between cells within a cortical column (Eckhorn *et al.*, 1988; Gray and Singer, 1989), in neighboring hypercolumns (Eckhorn *et al.*, 1988; Gray *et al.*, 1989), in distant hypercolumns (Gray *et al.*, 1989), and lying in two different cortical areas (Eckhorn *et al*, 1988). Stimulus position, orientation, movement direction, and velocity were among the stimulus properties that yielded stimulus-evoked resonances. Synchronized oscillatory responses were frequently found at distant cortical positions when at least one of the primary coding properties was similar.

While the whole of these results have received a great deal of attention, the most surprising findings (and the most difficult to explain) are those concerning the large spatial separations across which stimulus-evoked synchrony may occur. Using a single long moving bar stimulus, Gray *et al.* (1989) recorded simultaneously from cells which were separated by large cortical distances. Gray *et al.* found that for cortical separations great enough that the receptive fields of the cells did not overlap (> 2 mm), coherent oscillations occurred only between cells with similar orientation preferences. Even at these large separations, the cross-correlations of the firing patterns of the cells indicated a tight synchrony, on average having a 0 ms phase lag. Nearly all phase-locked cells showed activity peaks within 3 ms of each other. Thus assuming a 25 ms period of oscillation, phase differences were typically less than 12% of the period.

Gray *et al.* repeated this procedure using two short disconnected bars as the stimuli. At large recording distances, only one bar would pass through the receptive field of one cell, and exclusively the second bar would pass through the receptive field of a second cell. Yet when the two bars were moved colinearly in the same direction at the same speed, two distant cells frequently synchronized their oscillations even though there was a gap between the stimuli. When the bars were moved in opposite directions no synchrony resulted.

These stimulus-evoked resonances have been interpreted as reflecting the global properties of the stimulus. For instance, in the two bar stimulus paradigm, colinear but disconnected bars moving in the same direction at the same speed may be perceptually interpreted as a single continuous contour that is occluded in the middle, whereas two bars moving in opposite directions (without rotation) are likely to be perceptually interpreted as different contours. Segregation across occluding regions is a common problem that the visual system must solve regularly. In nature, occlusion may arise due to internal sources such as retinal veins in front of the photoreceptors or external sources such as a tree branch between the observer and the object of interest.

Until the present work was carried out, attempts to explain these oscillatory phenomena have typically been restricted to formal equations for the phase relations among abstractly defined oscillators (Atiya and Baldi, 1989; Baldi and Meir, 1990; Kammen, Holmes, and Koch, 1989). Herein we explain how suitably designed neural networks can give rise to such oscillations as an emergent property of their real-time dynamics. Moreover, we use neural networks which have previously been derived to explain and predict behavioral and neural data, other than the oscillatory phenomena themselves.

2. Theoretical Predictions of Visual Cortical Coding and Recognition Learning

Grossberg and Mingolla have developed a neural network theory of preattentive vision in which a new type of cortical cell, called a *bipole cell*, was predicted to exist (Grossberg, 1984, 1987a, 1987b; Grossberg and Mingolla, 1985a, 1985b, 1987). Bipole cells cooperatively link perceptual features into emergent boundary segmentations via cooperative-competitive feedback signals in a network called the CC Loop. The CC Loop is part of a larger neural model, called the Boundary Contour System (BCS), which suggested new perceptual roles

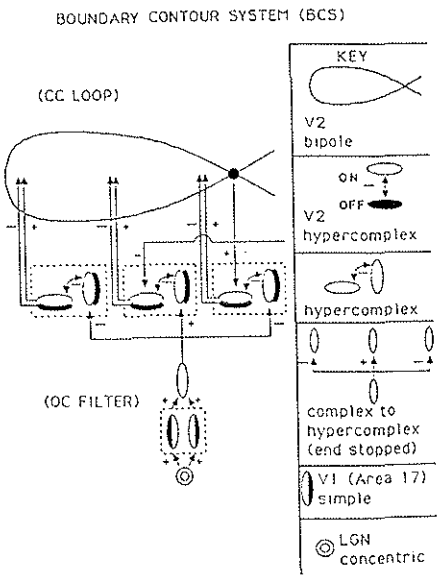

Figure 1. The static Boundary Contour System circuit described by Grossberg and Mingolla (1985a). The circuit is divided into an oriented contrast-sensitive filter (SOC Filter) followed by a cooperative-competitive feedback network (CC Loop). Multiple copies of this circuit are used, each corresponding to a different range of receptive field sizes of the SOC Filter. The depicted circuit has been used to analyse data about monocular vision. A binocular generalization of the circuit has also been described (Grossberg, 1987b; Grossberg and Marshall, 1989).

for cortical simple cells, complex cells, hypercomplex cells, and bipole cells (Figure 1). In addition, the BCS was used to explain and predict a variety of psychophysical and perceptual data, notably data about texture segregation, subjective contours, filling-in of brightness and color, and 3-D surface perception.

The bipole cell receptive field was predicted to consist of two long, thin independent flanks which non-linearly sum inputs from cells with orientation preferences similar to the orientation of the long axis of the bipole (Figure 2). Bipole cell output signals can be activated if and only if both flanks are sufficiently activated. These signals feed excitatory input back to model hypercomplex cells in a lower network layer which have the same orientation preference and are positioned near the middle of the bipole cell. Through this cooperative feedback cycle, two disconnected but colinear contours can induce a boundary completion between them.

Although the bipole cell was predicted on perceptual grounds, its existence was soon supported by neurophysiological data. Recording from area 18 of alert monkeys, von der Heydt *et al.* (1984) found cells that responded to moving illusory contours. That is, with no local luminance information to suggest a contour and only with colinear inducing lines lying beyond the receptive fields of the cells, cells responded strongly when the global percept of the stimulus suggested an illusory contour. When the stimulus was altered so that an illusory contour was no longer perceived, the cells did not respond. Inducing lines on both sides of the site were necessary for the perception of the illusory contours by both the cells and human observers. These data indicate that some cells in visual cortex respond well to subjective contours, and that cells which are not directly activated by bottom-up signals require input from at least two colinear flanking regions in order to be activated.

In addition to this electrophysiological data, Gilbert and Wiesel (1989) provided anatomical evidence from areas 17 and 18 of the cat. They remarked that "a prominent and stereotypical feature of cortical circuitry in the striate cortex is a plexus of long-range horizontal connections running for 6–8 mm parallel to the cortical surface." Using retrograde

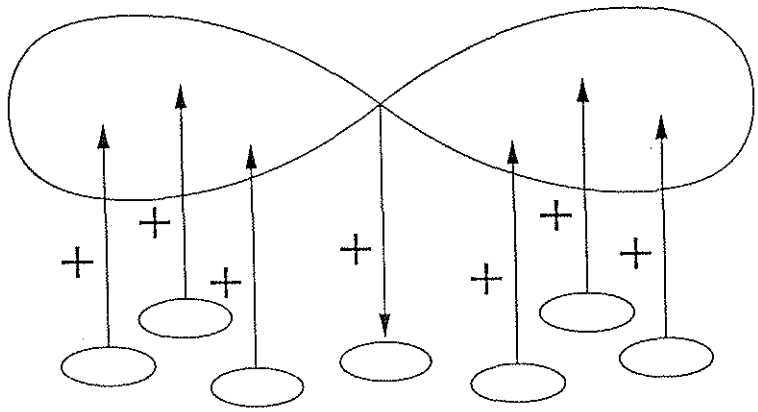

Figure 2: A bipole cell fires only if it is activated by sufficient input of similar orientation and/or direction to both of its receptive fields. It then delivers positive feedback signals to the layers of cells by which it was activated.

labeling, they found that these connections run between cortical columns of similar orientation preferences. Individual cells tended to have long and narrow receptive fields and greater than 90% of the connections appeared to be excitatory. Gilbert and Wiesel noted that while like orientation was necessary to achieve labelling, it was not sufficient. They speculated that there were "subthreshold contextual influences" at work. However, from these labeling techniques they were unable to determine a consistent relation between the orientation of the axis of the axonal fields and the orientation preferences of the columns to which they connected. While such evidence is not conclusive proof of the existence of long-range cooperative bipole cells in visual cortex, it does seem to strongly support the biological plausibility of the bipole mechanism.

In earlier modelling work on the dynamics of cortical coding, Grossberg (1976b, 1978c) predicted that cortical codes would be expressed by resonant standing waves in which cooperatively linked cells oscillate in phase with one another. It was also noted that these standing waves could be replaced by approach to an equilibrium point, or attractor, if no "slow" variables, such as inhibitory interneurons or chemical modulators, exist in the network. Both standing waves and equilibria can, in principle, support a feature-based cortical code. The standing waves were called "order-preserving limit cycles" to emphasize that the ordering, or relative importance, of feature detector activations should persist during each coding cycle, even if their absolute activations vary through time as the oscillation unfolds.

Mathematical analyses of both the standing wave and equilibrium point models were initiated in the 1970's. Studies of equilibrium point models led to a series of mathematical theorems, including a general theory for globally analysing equilibria and oscillations in competitive neural networks (Grossberg, 1978a, 1978b, 1980), and the Cohen-Grossberg model and theorem for content addressable memory (Cohen and Grossberg, 1983; Grossberg, 1982a). The Cohen-Grossberg model was designed to include the additive model, subsequently studied by Hopfield (1984), as well as the shunting model that describes interactions between cells that obey a membrane equation; see Grossberg (1988) for an historical overview. The present article continues the analysis of standing waves that was initiated in Ellias and Grossberg (1975).

The standing wave prediction was made in the context of a theory, called Adaptive Resonance Theory (ART), which analyses the role of reciprocal top-down and bottom-up

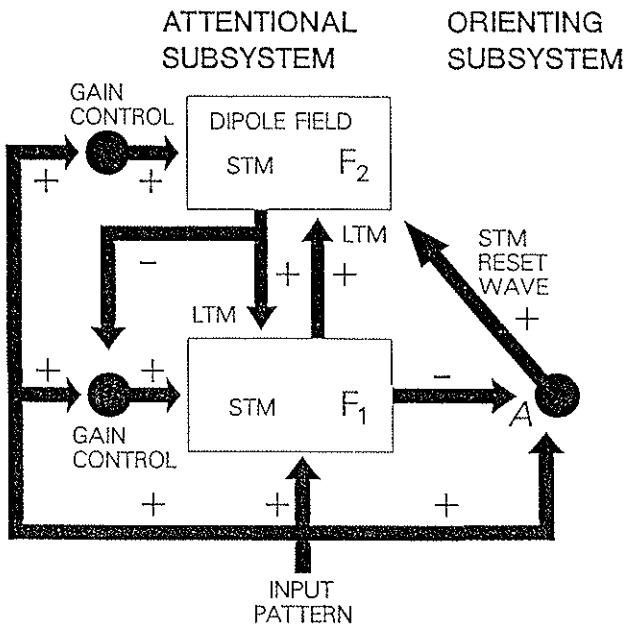

Figure 3. ART 1 system: Two successive stages, F_1 and F_2, of the attentional subsystem encode patterns of activation in short term memory (STM). Bottom-up and top-down adaptive filter pathways between F_1 and F_2 contain trainable long term memory (LTM) traces which multiply the signals in these pathways. The remainder of the circuit modulates these STM and LTM processes. Modulation by gain control enables F_1 to distinguish between bottom-up input patterns and top-down priming, or expectation, patterns, as well as to match these bottom-up and top-down patterns by the 2/3 Rule. Gain control signals also enable F_2 to react supraliminally to signals from F_1 while an input pattern is on. The orienting subsystem generates a reset wave to F_2 when sufficiently large mismatches between bottom-up and top-down patterns occur at F_1. This reset wave selectively and enduringly inhibits previously active F_2 cells until the input is shut off, and triggers a bout of hypothesis testing or memory search for a better F_2 representation.

cortico-cortical and thalamo-cortical adaptive filters in the development of cortical feature detectors, recognition learning, attentional processing, and memory search (Grossberg, 1976a, 1976b, 1978c, 1982b). Within ART, a resonant standing wave can occur when bottom-up and top-down signals fuse into an attentional focus. Such an attentional focus can support new learning as it gives rise to a conscious perceptual experience. The predicted linkage between standing waves, attention, and conscious experience has recently begun to attract the interest of a large number of investigators.

Mathematical investigations of complete ART architectures have heretofore tended to analyse equilibrium point models (Figure 3), wherein slow variables are eliminated for simplicity (Carpenter and Grossberg, 1987a, 1987b, 1990; Carpenter, Grossberg, and Reynolds, 1991). The present results illustrate how the ART standing waves predicted in Grossberg (1976b, 1978c) can be generated by the type of bottom-up and top-down feedback interactions among adaptive filters that are used in ART circuits.

The ART adaptive filter prediction was made before the BCS, or its cooperative bipole cells, were discovered. The present article demonstrates that both the CC Loop and ART circuits can cooperatively link cells into stimulus-specific standing waves wherein cell activities oscillate in phase with each other. More generally, we show that Cooperative Bipole Coupling, Adaptive Filter Coupling, Nearest Neighbor Coupling, and Random Connection Coupling can all generate the desired results. Thus, in preattentive visual segmentation, synchronous oscillations may reflect the binding of local feature detectors into a globally coherent grouping. In object recognition, synchronous oscillations may occur during an attentive resonant state that triggers new learning. The robust nature of the mathematical phenomenon is hereby demonstrated. Synchronized oscillations may be generated in different parts of the brain by circuits that carry out different functional tasks; in particular, preattentive vision and attentive visual object recognition. The existence of synchronized

oscillations in two different parts of the brain does not, in itself, imply that they carry out similar functions.

3. Specification of the Model

The source of the 40–60 Hz oscillations that have been reported has yet to be identified. With an average period of 16–25 ms, such oscillations may arise from local network effects, such as a feedback loop between an inhibitory interneuron and an excitatory cell, or the oscillations may be due to single cell membrane effects, such as the influence of a slow channel or second messenger. In the present simulations, we investigated how neural circuits that have already been shown to have strong behavioral and neural predictive value could act to synchronize their cell activations in a stimulus-specific manner.

The starting point for our work is the analysis by Ellias and Grossberg (1975) of oscillations within a neural network of excitatory potentials X_i and inhibitory interneuronal potentials Y_i which obey the equations

$$\frac{d}{dt}X_i = -AX_i + (B - X_i)[\sum_{k=1}^{n} f(X_k)C_{ki} + I_i] - X_i \sum_{k=1}^{n} f(Y_k)D_{ki} \tag{1}$$

and

$$\frac{d}{dt}Y_i = -EY_i + \sum_{k=1}^{n} X_k F_{ki}. \tag{2}$$

Each excitatory potential X_i in (1) obeys a membrane, or shunting, equation (Grossberg, 1973; Rall, 1955a, 1955b, 1956; Sperling and Sondhi, 1968), whereas each inhibitory interneuronal potential Y_i is approximated by an additive equation in (2). In equation (1), parameter A is the passive decay rate, B is the excitatory saturation point, C_{ki} is the excitatory path strength from cell k to cell i, I_i is an external input, and D_{ki} is the inhibitory path strength from cell k to cell i. In (2), parameter E is the passive decay rate, and F_{ki} is the excitatory path strength from cell k to cell i. A case of particular interest is the 2-dimensional E-G network

$$\frac{d}{dt}X = -AX + (B - X)(C[X - \Gamma]^+ I) - DX[Y - \Gamma]^+ \tag{3}$$

and

$$\frac{dY}{dt} = E(X - Y), \tag{4}$$

where $[w]^+ = \max(w, 0)$, which was shown (Ellias and Grossberg, 1975) to undergo a series of Hopf bifurcations from equilibrium to frequency-dependent oscillations as the arousal level I is parametrically increased. This input-dependent oscillatory behavior is representative of visual cortical neurons that fire repetitively only when stimulated.

The parameters used in the present simulations were chosen as follows: $A = 1$, $B = 1$, $C = 20$, $D = 33.3$, $\Gamma = 0.4$, $E = F = 0.025$. These values were prescribed in Ellias and Grossberg's original work. The choice $E = 0.025$ was made to give the oscillator strong relaxation properties due to the relative time scale differences between the passive decay rates A and E of the excitatory and inhibitory cells. These parameters also produce a desirable "spike-like" waveform. For these parameter choices, the $X - Y$ unit in (3) and (4) exhibited stable limit cycle oscillations for inputs between $I = 0.7$ and $I = 2.25$. The present results are consistent with the hypothesis that relaxation oscillators couple more rapidly and more reliably than sinusoidal oscillators for a variety of architectures (Somers and Kopell, 1991).

The simulations reported here utilized a one-dimensional array of 64 $X - Y$ units organized, as in Ellias and Grossberg (1975), in a ring to avoid boundary effects. In order to

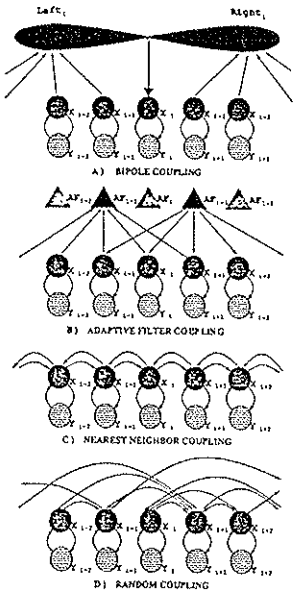

Figure 4: Coupling architectures. Figures A–D show the connectivities characteristic of the four coupling architectures implemented in the simulations. Each $X-Y$ pair represents a single oscillator and the lines indicate typical connections. In (A) the bowtie-shaped symbol represents a single bipole cell. Coupling inputs from the right of oscillator i feed exclusively into the right half of the bipole. Coupling inputs from the left feed exclusively into the left half of the bipole. The two halves of the bipole are combined and the rectified, thresholded coupling signal that results feeds to oscillator i. There is a single bipole cell corresponding to each $X-Y$ oscillator pair. In (B) the triangle-shaped symbols represent adaptive filter (AF) elements. Each adaptive filter element may receive coupling input from many oscillator units, and in turn may feed coupling output back to many oscillator units. In these simulations there are as many adaptive filter elements as there are oscillator units. In (C) each oscillator unit is connected reciprocally and equally with its immediate neighbor on either side and with no other oscillator units. In (D) each oscillator is connected with a fixed number of randomly chosen oscillators. All oscillators send out the same number of coupling outputs, but typically receive different numbers of coupling inputs. The filled arrowheads indicate excitatory connections, while unfilled arrowheads indicate inhibitory connections. The only inhibitory connections are from the Y cells to the X cells.

connect these oscillatory units, a cooperative feedback loop among the potentials X_i was implemented. Thus each excitatory-inhibitory unit (X_i, Y_i) in the array obeys the equations:

$$\frac{d}{dt}X_i = -AX_i + (B - X_i)(C[X_i - \Gamma]^+ + \alpha C[Z_i - \Gamma]^+ + I_i) - DX_i[Y_i - \Gamma]^+ \tag{5}$$

and

$$\frac{d}{dt}Y_i = -EY_i + FX_i. \tag{6}$$

In (5), Z_i is the activity of the ith coupling unit. This term will be specified below. Parameter α calibrates the size of the excitatory coupling strength relative to that provided by the self-excitatory term $C[X_i - \Gamma]^+$. In these simulations, α was parametrically increased from 0—the no-coupling case—to test the effects of excitatory interneuronal coupling on the coherence of the oscillations.

4. Cooperative Coupling Mechanisms

Several coupling architectures were investigated; namely, Cooperative Bipole Coupling, Adaptive Filter Coupling, Nearest Neighbor Coupling, and Random Connectivity Coupling (Figure 4). This analysis illustrates the robust nature of the synchrony phenomenon. Each coupling unit Z_i could be interpreted biologically as either the output signal from the dendritic tree of an X_i cell, or as another cell that sends an excitatory connection to the X_i cell.

For example, the Cooperative Bipole Coupling (Figure 4a) could be interpreted as a bipolar dendritic tree in which both compartments must be sufficiently activated to provide input to the X_i cell. Alternately, this coupling unit could be interpreted as a distant cell, perhaps lying in Area 18 (Grossberg and Mingolla, 1985a; von der Heydt, Peterhans, and Baumgartner, 1984), having the same dendritic properties and making a monosynaptic connection with the X_i cell. The coupling units are made explicit in the following equations:

Cooperative Bipole Coupling

$$Z_i = \left[\frac{P(\text{Right}_i)^n}{Q^n + (\text{Right}_i)^n} + \frac{P(\text{Left}_i)^n}{Q^n + (\text{Left}_i)^n} - \Gamma_{cpl}\right]^+ \tag{7}$$

where

$$\text{Right}_i = \frac{1}{\text{width}} \sum_{j=1}^{\text{width}} [X_{i+j} - \Gamma]^+ \tag{8}$$

and

$$\text{Left}_i = \frac{1}{\text{width}} \sum_{j=-1}^{-\text{width}} [X_{i+j} - \Gamma]^+. \tag{9}$$

Parameters P,Q, and n in (7) characterize a sigmoidal, or S-shaped, response curve that indicates a typical non-linear summation within each cell compartment (Grossberg, 1973, 1982b; Rall, 1955a, 1955b, 1956). For these simulations, the values $P = 1$,$Q = 0.10$, and $n = 5$ were chosen. Parameter Γ_{cpl} is the coupling threshold. The choice $\Gamma_{cpl} = P$ was made in order to guarantee that both compartments or flanks needed to be sufficiently activated before Z_i could be activated, and thus before coupling feedback from Z_i to X_i could be generated. The width of the flanks was parametrically varied in the simulations.

Adaptive Filter Coupling

$$Z_i = \left[\frac{1}{\text{fan out}} \sum_{j=-\text{fan out}/2}^{+\text{fan out}/2} AF_{i+j} - \Gamma_{cpl}\right]^+ \tag{10}$$

where

$$AF_i = \frac{1}{\text{fan in}} \sum_{j=-\text{fan in}/2}^{+\text{fan in}/2} [X_{i+j} - \Gamma]^+. \tag{11}$$

The Adaptive Filter coupling (Figure 4b) assumes that many inputs fan-in, bottom-up, to each coupling compartment AF_i, and that these AF_i's fan-out, top-down, to many compartments Z_i. In the general case (fan in > 1, fan out > 1), this coupling can be realized, for example, by letting each Z_i collect signals in the excitatory dendritic tree that feeds X_i. In the case fan out $= 1$, AF_i and Z_i may be collapsed into the same dendritic structure, and it is not necessary to postulate intervening cells.

Nearest Neighbor Coupling

$$Z_i = 1/2[X_{i-1} - \Gamma]^+ + 1/2[X_{i+1} - \Gamma]^+ \tag{12}$$

Nearest Neighbor coupling (Figure 4c) is defined by excitatory signalling between each cell and its two immediate neighbors.

Random Connection Coupling

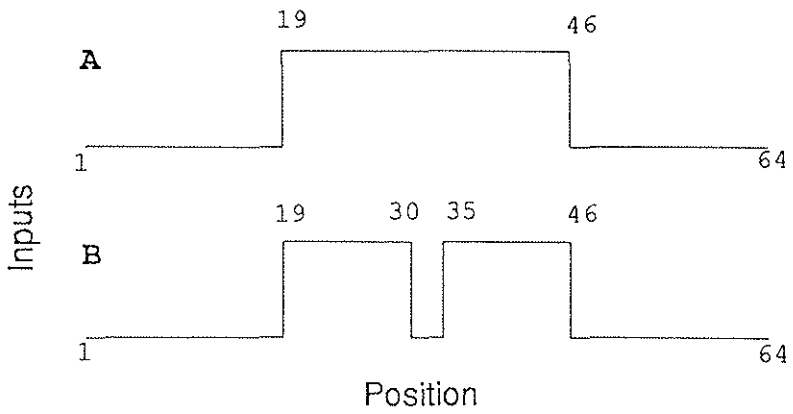

Figure 5: Single bar and double bar system inputs. Simulations were run on two different input images: a single, long bar (A); or two short bars separated by a slit (B). The values of I_i are displayed for each position i along the 64-position ring. Each high value ($I_i = 1.0$) represents a position on a bar in the image and is sufficient to drive an uncoupled $X - Y$ pair into its oscillatory regime. Each low value $I_i = 0.05$ represents part of the background of the image and is not sufficient to drive oscillations in an uncoupled $X - Y$ pair; rather, an equilibrium value is approached. Within the course of a simulation run, all input values were constant and did not themselves oscillate.

$$Z_i = \Big[\frac{1}{\text{num conn}} \sum_{\text{random } j}^{\text{num conn}} [X_{i+j} - \Gamma]^+ - \Gamma_{cpl}\Big]^+. \qquad (13)$$

Random coupling (Figure 4d) sums the active inputs of a number of random connections. If the total input is sufficiently great, an excitatory signal to X_i is activated. Note that while the coupling is chosen randomly, the same random connections remain in effect throughout the course of a simulation run.

5. Methods

The typical paradigm for the simulations is as follows. At the start of each simulation, the $X - Y$ units were given random initial conditions and the coupling variables Z were set equal to zero. The test stimuli were either long single bar images or short disconnected double bar images (Figure 5). For the single bar stimulus, the central region ($i = 19$ to $i = 46$) was set to the target value. The double bar stimulus differed in that a central slit region ($i = 31$ to $i = 34$) was set to the background value. Input array positions corresponding to part of a bar were given values sufficient to generate stable limit cycle oscillations in an uncoupled unit [equations (3) and (4)]. At positions not on a bar, the input value was insufficient to sustain oscillations in its unit. For a given simulation run, the inputs and parameters were chosen and held fixed. Within a series of runs, a parameter or pair of parameters, such as the synaptic coupling strength α and/or the widths of coupling interaction, were varied in order to determine their effects. The simulations were written in C and run on a Silicon Graphics IRIS/4D. The ordinary differential equations were numerically integrated using a standard published Adaptive-Stepsize Runge-Kutta routine (4th order) (Press *et al.*, 1988). Critical results were checked using a published Rational Function Extrapolation method (Bulirsch-Stoer) (Press *et al.*, 1988). Since these methods arrive at their results by fundamentally different techniques, when both methods yield the same result it is highly unlikely that numerical error had a significant effect on the results.

6. Results

The primary control experiment for these simulations is the uncoupled ($\alpha = 0$) case. In the uncoupled case, units receiving sufficient input exhibit stable limit-cycle oscillations, while units receiving insufficient input quickly approach a low equilibrium value (Figures 6 and 7). Since the initial values were chosen randomly, the units oscillated in random phase with respect to one another. If all ON inputs were the same, these phase relationships did not change over the time course of the simulation, since their frequencies were the same.

Using the Cooperative Bipole Coupling Architecture in (7)–(9), coherent oscillations emerged rapidly (approximately one cycle or less) for both the one bar (Figure 8) and two bar (Figure 9) stimuli. In the two bar case, oscillations were induced in the slit between the two bars and these oscillators could be almost instantly synchronized with the others. In both stimulus cases, the bipole architectures did not induce a spreading of oscillatory activity to the outer regions beyond the stimuli. Inward boundary completion without outward spreading of oscillatory activity was found to be a robust property of bipole coupling.

Adaptive Filter coupling also yielded rapid synchronization for single bar stimuli (Figure 10). As shown in Figure 11, the disconnected regions that were activated by a double bar stimulus were synchronized with respect to each other. This is a robust property of adaptive filter coupling. If the fan-in and fan-out are chosen broadly enough to only include one bar, then the cellular units corresponding to that bar become synchronized. If the fan-in and fan-out are chosen broadly enough to also include the region spanned by both bars, then units corresponding to both bars are synchronized. Depending upon cell parameters, the intervening units may undergo synchronized subthreshold or suprathreshold oscillations. There is also a strong tendency for cells flanking the exteriors of the bars to undergo analogous oscillations.

Nearest neighbor coupling (Figure 12) and random coupling (Figure 13) could also cause coherent oscillations to emerge, although this synchrony did not occur as rapidly, nor for as robust a set of initial conditions, as it did for the bipole and adaptive filter architectures. Selective boundary completion was not a feature of either the nearest neighbor or random couplings. Disconnected bars could still be synchronized under suprathreshold conditions, but then the oscillation spread from each bar in both directions. For nearest neighbor coupling this occured only for small slit widths (4 or fewer positions).

Figures 7 and 9 together with Figures 14 and 15 present two different perspectives of the synchronized behavior for double bar stimulus, using the bipole architecture. Figures 7 and 14 display the uncoupled ($\alpha = 0$) case and Figures 9 and 15 display the tight synchrony ($\alpha = 0.25$) of the bipole coupling. Not only are the two bars synchronized, but also synchronized oscillations were induced in the slit region between the two bars, indicating that a subjective contour was perceived across the slit and that the features were linked across the "occluding" region, as was also ascribed to bipole cells in the equilibrium point version of the BCS (Grossberg and Mingolla, 1985a, 1985b).

The coherence of the oscillations is measured quantitatively by the standard deviation of the phases along the stimuli over time. Figure 16 displays the emerging synchrony of the bipole architecture as the coupling strength α in (5) increases. The sample standard deviation of the phases is computed at each peak and trough over the time course of the simulation. The effects of the coupling strengths can thus be compared on a single graph.

As the coupling strength α is increased from 0 over a series of runs, the oscillations become increasingly coherent. For instance, in the double bar case, at a low coupling strength the oscillators along each bar begin to synchronize but the two bars are out of phase with

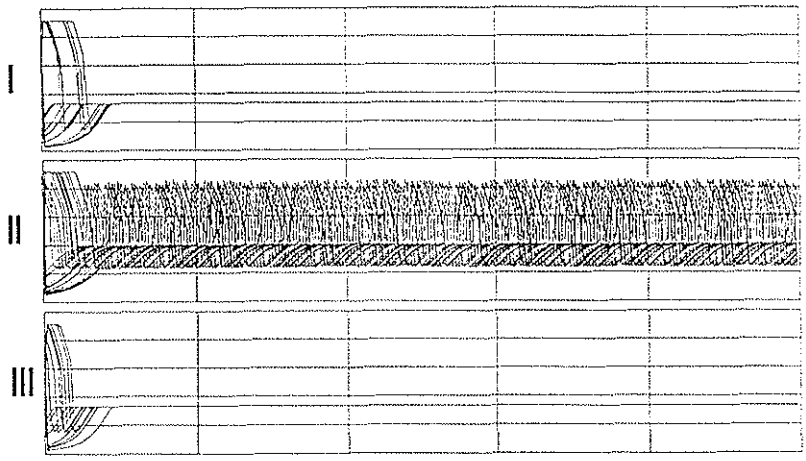

Figure 6: Uncoupled ($\alpha = 0$) case for single bar input. Three windows are displayed in which plots of X_i versus time are overlayed. In window I, positions $i = 1$ thru $i = 18$ are overlayed. In window II, positions $i = 19$ thru $i = 46$ are plotted. Positions $i = 47$ thru $i = 64$ are shown in window III. The positions displayed in windows I and III correspond to the image background, while window II displays activity of X_i along the bar. In this uncoupled case, the activities at positions corresponding to the background quickly approach the same steady-state value, while positions along the bar oscillate in random phase. This uncoupled case represents the control simulation for single bar input.

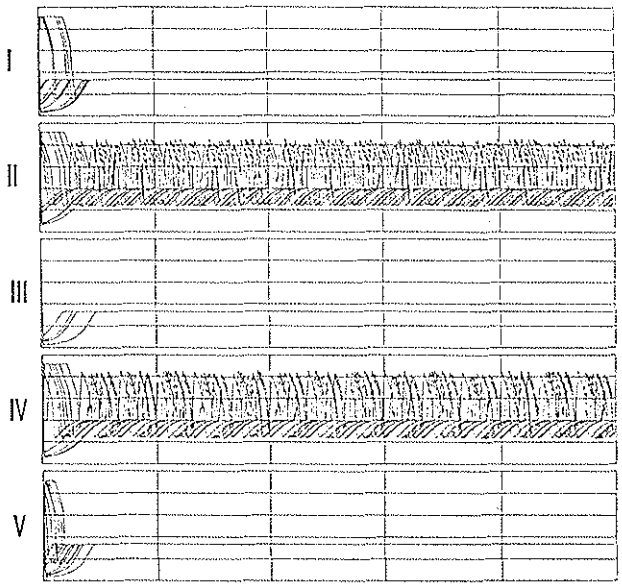

Figure 7: Uncoupled ($\alpha = 0$) case for double bar input. Five windows are displayed in which plots of X_i versus time are overlayed. In window I, positions $i = 1$ thru $i = 18$ are overlayed, while in window II, positions $i = 19$ thru $i = 30$ are plotted. Windows III and IV display positions $i = 31$ thru $i = 34$ and $i = 35$ thru $i = 46$, respectively, and positions $i = 47$ thru $i = 64$ are shown in window V. The positions displayed in windows I and V correspond to the image background, while window III displays activity in the slit between the two bars. Windows II and IV display activity of X_i along the left and right bars respectively. In this uncoupled case, the activities at positions corresponding to the background and the slit quickly approach the same steady-state value, while the activities at positions along both bars oscillate in random phase. This uncoupled case represents the control simulation for double bar input.

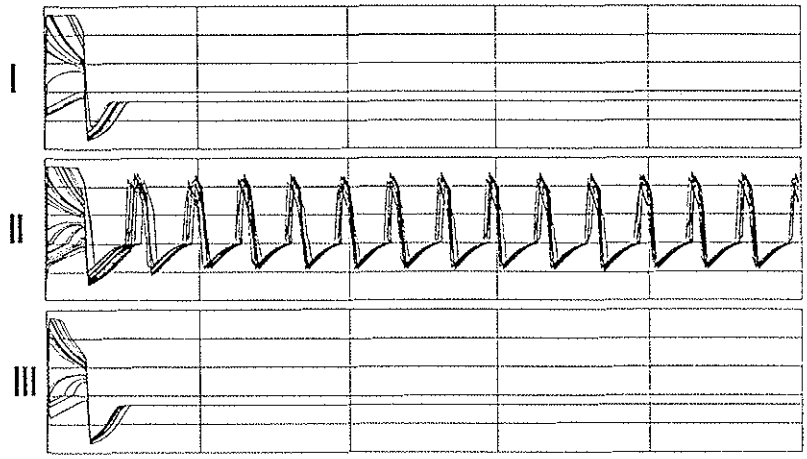

Figure 8: Bipole coupling for single bar input. Using the same inputs and initial conditions which were used to generate Figure 6, bipole coupling with $\alpha = 0.25$ yielded rapid and sustained synchronization of oscillatory activity at positions along the bar without inducing oscillatory activity at positions corresponding to the background. Each bipole flank received input from six neighboring positions (width = 6).

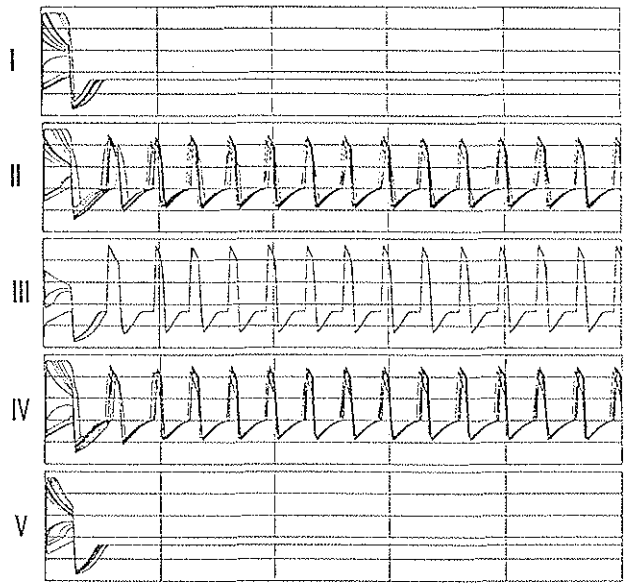

Figure 9: Bipole coupling for double bar input. Using the same inputs and initial conditions which were used to generate Figure 7, bipole coupling with $\alpha = 0.25$ yielded rapid and sustained synchronization of oscillatory activity at positions along both bars and induced synchronous oscillatory activity at the slit positions $i = 31$ thru $i = 34$ but did not induce oscillatory activity at positions corresponding to the outer background regions. This may be interpretted as the completion of a disconnected image boundary, resulting in the perception of a single long bar. Each bipole flank received input from six neighboring positions (width=6).

respect to one another and the bar ends may be asynchronous. At this strength, no oscillations yet occur in the slit region between the bars. As α increases, oscillations are induced in the slit. These oscillators lag behind the others in phase. Also at this strength, the oscillators along the bars become slightly less coherent for the first few cycles as the two bars begin to synchronize with respect to each other rather than just internally. As the coupling strength is further increased, the phase lag between the slit and the bars becomes negligible and the bar ends synchronize. The bars assume a more coherent relationship and do so more

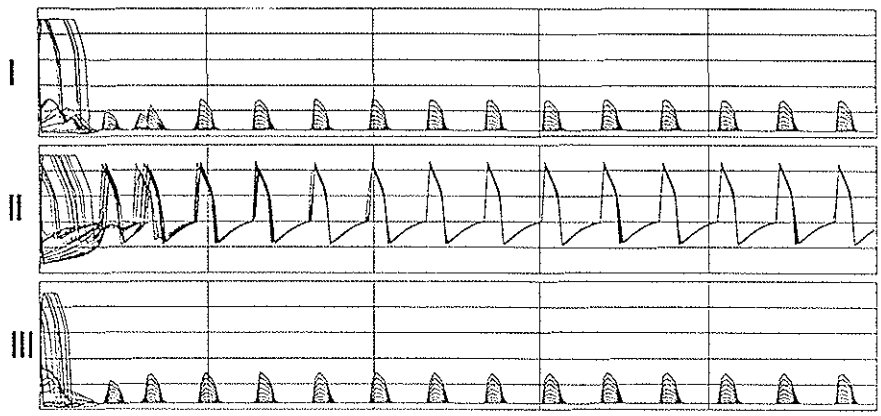

Figure 10: Adaptive filter coupling for single bar input. Shown here with $\alpha = 0.10$ and fan-in and fan-out widths of 9, adaptive filter coupling yielded rapid synchronization of oscillatory activity along the bar. While some small oscillatory activity was induced at background positions, this activity was well below the firing threshold of 0.4. The inputs and initial conditions were identical to those used in generating Figure 6.

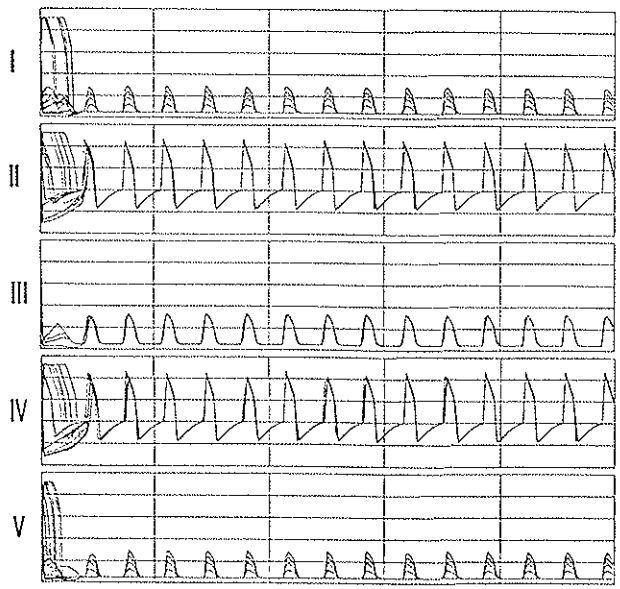

Figure 11: Adaptive filter coupling for double bar input. Shown here with $\alpha = 0.10$ and fan-in and fan-out widths of 9, adaptive filter coupling yielded rapid synchronization of oscillatory activity along each bar and synchronized the bars with respect to each other. While some small oscillatory activity was induced at background positions and in the slit, this activity was subthreshold. The inputs and initial conditions were identical to those used in generating Figure 7.

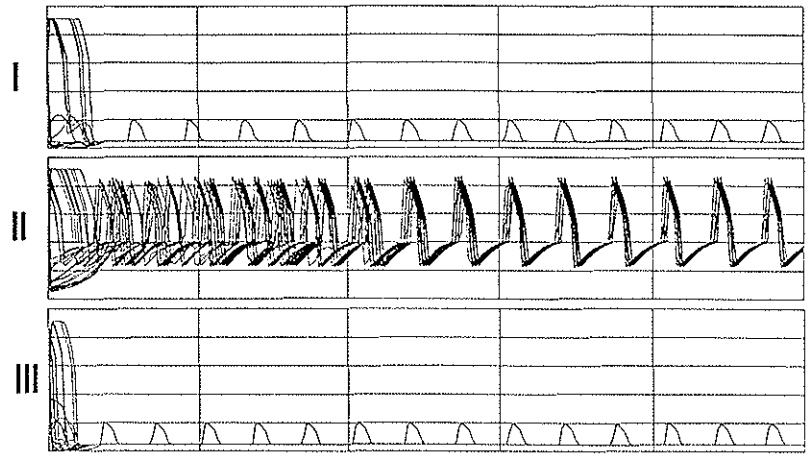

Figure 12: Nearest neighbor coupling for single bar input. Coherent oscillations are shown here to emerge rapidly (about six cycles) with only coupling between nearest neighbors ($\alpha = 0.05$).

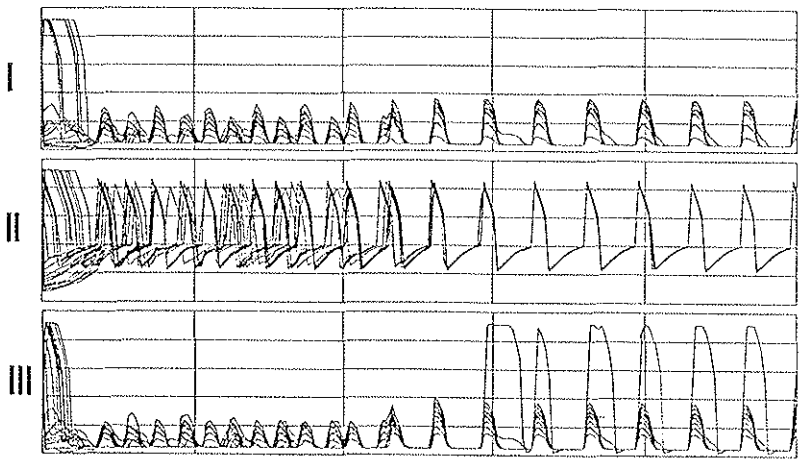

Figure 13: Random coupling for single bar input. Coherent oscillations rapidly emerged at positions along the bar stimulus for a random coupling shown here with $\alpha = 0.1$. Each X_i provided input to six other units, chosen randomly. These random connections remained fixed throughout the simulation. Since connections were random some units received input from more than six units while others received less. In window III oscillatory activity is induced in one unit which received more than six inputs. All other background units exhibited only subthreshold oscillations.

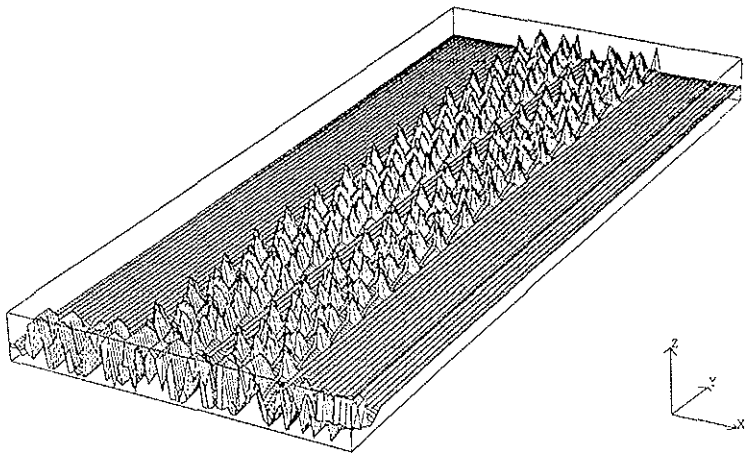

Figure 14: 3-D perspective of uncoupled case for double bar input. The data of Figure 7 is replotted in three dimensions in order to demonstrate the positional structure of the activity. The X-axis represents the position, i, of the $X - Y$ unit; the Y-axis represents time; and the Z-axis represents the activity, X_i. This perspective more clearly displays two regions of incoherent oscillatory activity separated by a slit of region that quickly approaches equilibrium. The larger background regions to the outsides also quickly approach equilibrium from their random initial conditions.

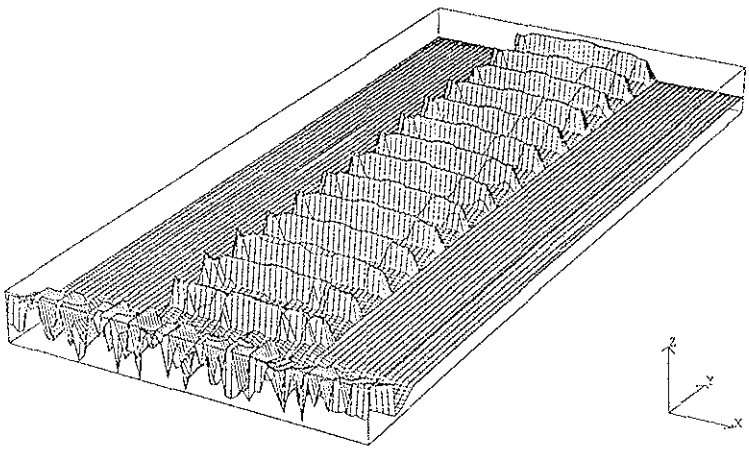

Figure 15: 3-D perspective of bipole coupling for double bar input. By implementing bipole coupling for the inputs and initial conditions shown in Figure 14, two nearby regions of incoherent oscillatory activity are very rapidly synchronized and oscillations are induced in the slit region and these oscillations very rapidly synchronize with the bar regions. This represents a successful boundary completion between the bars which results in a single coherent contour of oscillatory activity that does not spread to the outer background positions. The data plotted is the same that is shown in the overlay plots of Figure 9.

rapidly until the whole stimulus and slit region synchronizes together on the first cycle. The coherence of the oscillators continues to improve until the coupling input is so great that it drives the units out of their oscillatory regimes to a high equilibrium value. This effect is called oscillator death (Ermentrout and Kopell, 1990) and it is a typical phenomena among neural oscillators (Ellias and Grossberg, 1975). Analogous properties were found for all four

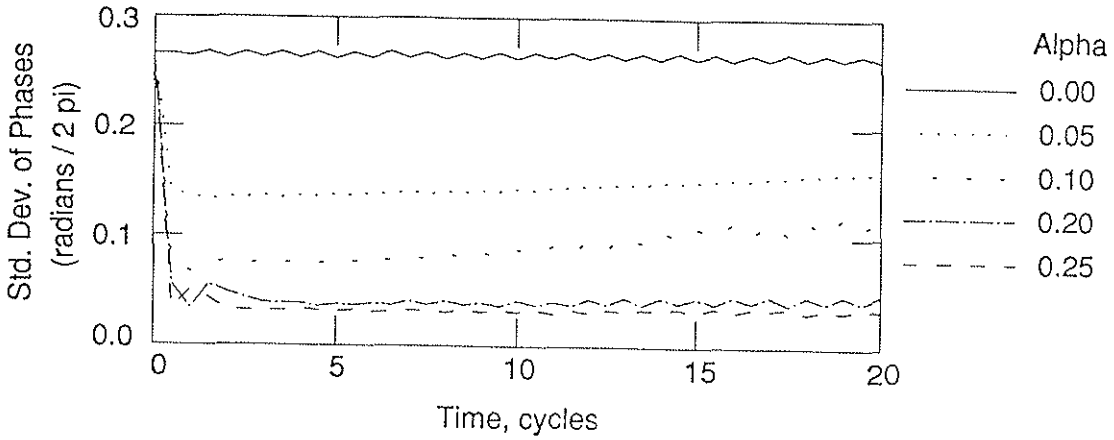

Figure 16: The population standard deviations of phases along the stimulus region over time for a range of coupling strengths. The standard deviations drop as the coupling strength increases. For $\alpha = 0.25$ a stable standard phase deviation of 0.03 is achieved. Such a value is well within the 12% deviation limit found experimentally by Gray *et al.* (1989). Parameter $\alpha = 0.20$ also falls within this limit with a standard phase deviation of less than 0.05. Oscillator death occurs at $\alpha = 0.30$.

types of models.

An interesting property is a bowing in phase that the bipole architecture has a tendency to induce. Although the first cycle of the oscillators may be synchronized, the bipole provides more input longer along the middle of the bar than at the ends. The middle of the bar thus tends to stay on longer. This property is minimized with relaxation oscillators, and is then negligible.

7. Discussion

The present results indicate that a wide variety of nonlinear cooperative feedback networks, whose cell units obey shunting or additive equations, can undergo synchronous oscillations if their coupling strength is sufficiently high, and if at least one slow variable, here a slow inhibitory interneuron, exists. These synchronous oscillations can, for example, support a preattentive boundary completion process, as occurs during visual boundary segmentation; an attentive resonant state, as occurs during visual object recognition; either preattentive or attentive adaptive filtering operations during more general processes of cortical feature detection and short term memory representation; or more abstract couplings by nearest neighbors or random connections.

Many researchers have recently focussed almost exclusively upon the existence of these synchronous oscillations. Now that the robust nature of the synchrony phenomenon has been demonstrated, a finer analysis of individual parametric features peculiar to the perceptual or cognitive codes supported by the oscillations can be carried out.

REFERENCES

Atiya, A. and Baldi, P. (1989). Oscillations and synchronizations in neural networks: An exploration of the labeling hypothesis. *International Journal of Neural Systems*, **1**, 103–124.

Baldi, P. and Meir, R. (1990). *Neural Computation*, in press.

Carpenter, G.A. and Grossberg, S. (1987a). A massively parallel architecture for a self-organizing neural pattern recognition machine. *Computer Vision, Graphics, and Image Processing*, **37**, 54–115.

Carpenter, G.A. and Grossberg, S. (1987b). ART 2: Stable self-organization of pattern recognition codes for analog input patterns. *Applied Optics*, **26**, 4919–4930.

Carpenter, G.A. and Grossberg, S. (1990). ART 3: Hierarchical search using chemical transmitters in self-organizing pattern recognition architectures. *Neural Networks*, **3**, 129–152.

Carpenter, G.A., Grossberg, S., and Reynolds, J.H. (1991). ARTMAP: Supervised real-time learning and classification of nonstationary data by a self-organizing neural network. *IEEE Expert*, in press.

Cohen, M.A. and Grossberg, S. (1983). Absolute stability of global pattern formation and parallel memory storage by competitive neural networks. *IEEE Transactions on Systems, Man, and Cybernetics*, **SMC-13**, 815–826.

Cohen, M.A. and Grossberg, S. (1984). Neural dynamics of brightness perception: Features, boundaries, diffusion, and resonance. *Perception and Psychophysics*, **36**, 428–456.

Eckhorn, R., Bauer, R., Jordan, W., Brosch, M., Kruse, W., Munk, M., and Reitbock, H.J. (1988). Coherent oscillations: A mechanism of feature linking in the visual cortex? *Biological Cybernetics*, **60**, 121–130.

Ellias, S.A. and Grossberg, S. (1975). Pattern formation, contrast control, and oscillations in the short term memory of shunting on-center off-surround networks. *Biological Cybernetics*, **20**, 69–98.

Ermentrout, G.B. and Kopell, N. (1990). Oscillator death in systems of coupled neural oscillators. *SIAM Journal of Applied Mathematics*, **50**, 125–146.

Gilbert, C.D., and Wiesel, T.N. (1989). Columnar specificity of intrinsic horizontal and corticocortical connection in cat visual cortex. *Journal of Neuroscience*, **9**, 2432–2442.

Gray, C.M., and Singer, W. (1989). Stimulus-specific neuronal oscillations in orientation columns of cat visual cortex. *Proceedings National Academy of Sciences (USA)*, **86**, 1698–1702.

Gray, C.M., Konig, P., Engel, A., and Singer, W. (1989). Oscillatory responses in cat visual cortex exhibit inter-columnar synchronization which reflects global stimulus properties. *Nature*, **338**, 334–337.

Grossberg, S. (1973). Contour enhancement, short-term memory, and constancies in reverberating neural networks. *Studies in Applied Mathematics*, **52**, 217–257.

Grossberg, S. (1976a). Adaptive pattern classification and universal recoding, I: Parallel development and coding of neural feature detectors. *Biological Cybernetics*, **23**, 121–134.

Grossberg, S. (1976b). Adaptive pattern classification and universal recoding, II: Feedback, expectation, olfaction, and illusions. *Biological Cybernetics*, **23**, 187–202.

Grossberg, S. (1978a). Decisions, patterns, and oscillations in the dynamics of competitive systems with applications to Volterra-Lotka systems. *Journal of Theoretical Biology*, **73**, 101–130.

Grossberg, S. (1978b). Competition, decision, and consensus. *Journal of Mathematical Analysis and Applications*, **66**, 470–493.

Grossberg, S. (1978c). A theory of visual coding, memory, and development. In **Formal theories of visual perception**, E. Leeuwenberg and H. Buffart (Eds.). New York: Wiley.

Grossberg, S. (1980). Biological competition: Decision rules, pattern formation, and oscillations. *Proceedings of the National Academy of Sciences*, **77**, 2338–2342.

Grossberg, S. (1982a). Associative and competitive principles of learning and development: The temporal unfolding and stability of STM and LTM patterns. In **Competition and cooperation in neural networks**, S.I. Amari and M. Arbib (Eds.). New York: Springer-Verlag.

Grossberg, S. (1982b). **Studies of mind and brain: Neural principles of learning, perception, development, cognition, and motor control**. Boston: Reidel Press.

Grossberg, S. (1984). Outline of a theory of brightness, color, and form perception. In **Trends in mathematical psychology**, E. Degreef and J. van Buggenhaut (Eds.). Amsterdam: Elsevier/North-Holland, pp. 59–86.

Grossberg, S. (1987a). Cortical dynamics of three-dimensional form, color, and brightness perception, I: Monocular theory. *Perception and Psychophysics*, **41**, 87–116.

Grossberg, S. (1987b). Cortical dynamics of three-dimensional form, color, and brightness perception, II: Binocular theory. *Perception and Psychophysics*, **41**, 117–158.

Grossberg, S. (1988). Nonlinear neural networks: Principles, mechanisms, and architectures. *Neural Networks*, **1**, 17–61.

Grossberg, S. and Marshall, J. (1989). Stereo boundary fusion by cortical complex cells: A system of maps, filters, and feedback networks for multiplexing distributed data. *Neural Networks*, **2**, 29–51.

Grossberg, S. and Mingolla, E. (1985a). Neural dynamics of perceptual grouping: Textures, boundaries, and emergent segmentations. *Perception and Psychophysics*, **38**, 141–171.

Grossberg, S. and Mingolla, E. (1985b). Neural dynamics of form perception: Boundary completion, illusory figures, and neon color spreading. *Psychological Review*, **92**, 173–211.

Grossberg, S. and Mingolla, E. (1987). Neural dynamics of surface perception: Boundary webs, illuminants, and shape-from-shading. *Computer Vision, Graphics, and Image Processing*, **37**, 116–165.

Kammen, D.M., Holmes, P.J. and Koch, C. (1989). Cortical architecture and oscillations in neuronal networks: Feedback versus local coupling. In **Models of brain function**, R.M.J. Cotterill (Ed.). Cambridge: Cambridge University Press.

Press, W.H., Flannery, B.P., Teukolsky, S.A., and Vetterling, W.T. (1988). **Numerical recipes in C: The art of scientific computing**. Cambridge: Cambridge University Press, pp. 566–597.

Rall, W. (1955a). A statistical theory of monosynaptic input-output relations. *Journal of Cellular and Comparative Physiology*, **46**, 373-411.

Rall, W. (1955b). Experimental monosynaptic input-output relations in the mammalian spinal cord. *Journal of Cellular and Comparative Physiology*, **46**, 413–437.

Rall, W. (1956). Analysis of reflex variability in terms of partially correlated excitability fluctuation in a population of motoneurons. *Journal of General Physiology*, **39**, 397–422.

Somers, D. and Kopell, N. (1991). Relaxation versus sinusoidal oscillators: Properties of oscillators affect emergent properties of networks. In preparation.

Sperling, G. and Sondhi, M.M. (1968). Model for visual luminance discrimination and flicker detection. *Journal of the Optical Society of America*, **58**, 1133–1145.

von der Heydt, R., Peterhans, E. and Baumgartner, G. (1984). Illusory contours and cortical neuron responses. *Science*, **224**, 1260–1262.